

Waveguides for Rydberg excitons in Cu_2O from strain traps

Sjard Ole Krüger* and Stefan Scheel

Institut für Physik, Universität Rostock, Albert-Einstein-Straße 23, D-18059 Rostock, Germany

(Dated: November 14, 2018)

We investigate the formation of waveguides for Rydberg excitons in Cu_2O from cylindrical stressors as alternatives to optical traps. We show that the achievable potential depths can easily reach the meV and the trap frequencies the GHz regimes. For Rydberg excitons, we find that it is sufficient to consider only the shift of the band gap, whereas the excitonic binding energies remain almost unchanged.

PACS numbers: 78.20.Bh, 71.35.-y, 71.70.Fk

I. INTRODUCTION

Excitons, bound states of an electron and a positively charged hole, are the fundamental optical excitations in a semiconductor. Cuprous oxide (Cu_2O) was the first material in which the formation of excitons with principal quantum numbers up to $n = 8$ was experimentally demonstrated^{1,2}. In recent years, the variety of observed excitonic states has increased greatly³⁻⁵, including highly excited states of principal quantum numbers up to $n = 25$ and orbital quantum numbers of $\ell = 5$. These highly excited states do already show all the hallmarks of the Rydberg blockade³ as well as signs of quantum coherence⁶.

Strain potentials from inhomogeneous strain fields alter the band structure of the crystal and can generate effective trapping potentials. They have been used and extensively investigated in the pursuit of exciton condensation in Cu_2O ⁷⁻¹³. Due to the long lifetime of the 1S paraexciton of its yellow exciton series ($\sim \mu\text{s}$), most research has hitherto been focused on the yellow 1S para- and orthoexcitons. Strain influence on the yellow P-excitons has been investigated in thin films¹⁴. In comparison to the dipole traps frequently used in atomic physics, strain traps potentially offer a greater variety of achievable trap geometries, as the shape of the trap depends strongly on the shape of the stressor, the stress applied to it, the excitonic state in question as well as the orientation of the crystal relative to the stress^{10,15}. Furthermore, the achievable potential depths ($\sim \text{meV}$) and trap frequencies ($\sim \text{GHz}$) are much higher than those of the atomic dipole traps ($\sim \mu\text{eV}$ and $\sim \text{MHz}$)¹⁶.

Excitonic traps may be a useful experimental tool for the investigation of exciton-exciton interactions and many-body effects in exciton populations. The 1D potential landscapes induced by cylindrical stressors offer a positional control over the exciton populations in two dimensions and could pave the way for the investigation of 1D many-body interactions between excitons.

In this article, we investigate the modification of the Rydberg exciton resonances in Cu_2O under the influence of strain from a cylindrical stressor (see Fig. 1). The strain field $\epsilon(\mathbf{r})$ will be calculated using Hertzian contact theory^{17,18}, while the band Hamiltonian derived by Suzuki and Hensel¹⁹ will be employed in order to describe

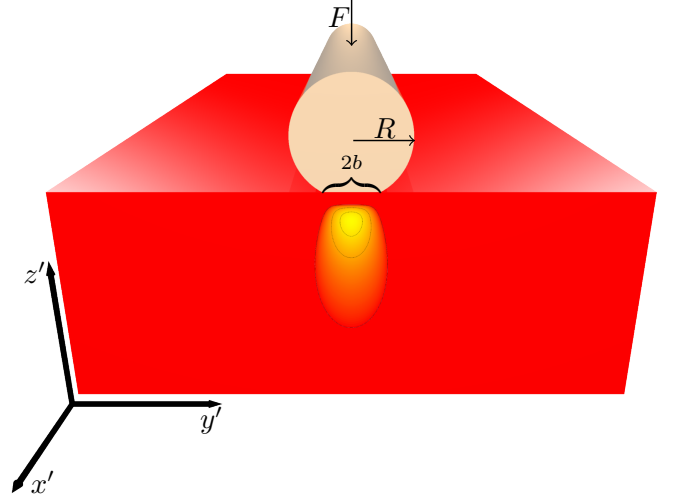


FIG. 1. Schematic cross section of the proposed geometry with a cylindrical stressor acting on a Cu_2O crystal with line load F (force per unit length) and the resulting trapping potential. b denotes the half width of the contact area.

the strain dependence of the hole motion, from which the band-gap shifts $\Delta E_g(\mathbf{r})$ can be obtained. The shifts of the binding energies will be calculated using a two-band model similar to Ref.⁵, generalised to anisotropic band structures.

The article is organised as follows. Section II introduces the band and strain Hamiltonians used in this study. In Sec. III the strain fields and the resulting band-gap shifts will be calculated for certain geometries and stresses. The influence on the excitonic binding energies will be discussed in Sec. IV, and Sec. V presents the conclusion and an outlook.

II. ELECTRON AND HOLE MOTION UNDER THE INFLUENCE OF STRAIN

We begin with a brief review of the band structure of Cu_2O under the influence of strain. Without spin, the uppermost valence band of Cu_2O has Γ_5^+ -symmetry at the zone center, which splits into a twofold degenerate Γ_7^+ - and a fourfold degenerate Γ_8^+ -band under the

influence of spin-orbit interaction. An effective 6×6 -Hamiltonian for these valence bands up to second order in the hole momentum $\hbar\mathbf{k}_h$ and first order in the components of the strain tensor ϵ_{ij} ($i, j = x, y, z$) can be constructed based on group-theoretical considerations¹⁹. It takes the form $\mathcal{H}_v(\mathbf{k}_h, \boldsymbol{\epsilon}) = \mathcal{H}_{so} + \mathcal{H}_{k_h} + \mathcal{H}_{\boldsymbol{\epsilon}}$ where $\mathcal{H}_{so} = -\frac{\Delta}{3}(2 + \mathbf{I} \cdot \boldsymbol{\sigma})$ describes the \mathbf{k}_h -independent spin-orbit splitting, \mathbf{I} denotes the vector of the angular-momentum matrices for $I = 1$, $\boldsymbol{\sigma}$ the vector of the Pauli matrices and Δ the spin-orbit splitting. Note that our definition of the spin-orbit splitting guarantees that the band edge of the Γ_7^+ valence band is located at the origin of the energy scale.

The \mathbf{k}_h -dependent part of the Hamiltonian is given by

$$\begin{aligned} \mathcal{H}_{k_h} = & \frac{\hbar^2}{2m_e} \left\{ (A_1 + B_1 \mathbf{I} \cdot \boldsymbol{\sigma}) \mathbf{k}_h^2 \right. \\ & + \left[A_2 \left(I_x^2 - \frac{1}{3} \mathbf{I}^2 \right) + B_2 \left(I_x \sigma_x - \frac{1}{3} \mathbf{I} \cdot \boldsymbol{\sigma} \right) \right] k_{x,h}^2 + \text{c.p.} \\ & \left. + [A_3(I_x I_y + I_y I_x) + B_3(I_x \sigma_y + I_y \sigma_x)] \{k_{x,h} k_{y,h}\} + \text{c.p.} \right\} \end{aligned} \quad (1)$$

where c.p. denotes cyclic permutations, $\{k_i k_j\} = (k_i k_j + k_j k_i)/2$ is the symmetric product of momenta, and the A_i and B_i are dimensionless material constants. Values for all material properties of Cu_2O used in this work can be found in Table I. In the absence of external electromagnetic fields, the symmetric, cartesian strain tensor $\boldsymbol{\epsilon}$ with components ϵ_{ij} transforms according to the same reducible representation of the point group O_h as $k_i k_j$, hence the strain Hamiltonian for the valence band has an analogous form to \mathcal{H}_{k_h}

$$\mathcal{H}_{\boldsymbol{\epsilon}} = (D_1 + E_1 \mathbf{I} \cdot \boldsymbol{\sigma}) \text{Tr}(\boldsymbol{\epsilon})$$

$$\begin{aligned} & + \left[D_2 \left(I_x^2 - \frac{1}{3} \mathbf{I}^2 \right) + E_2 \left(I_x \sigma_x - \frac{1}{3} \mathbf{I} \cdot \boldsymbol{\sigma} \right) \right] \epsilon_{xx} + \text{c.p.} \\ & + [D_3(I_x I_y + I_y I_x) + E_3(I_x \sigma_y + I_y \sigma_x)] \epsilon_{xy} + \text{c.p.} \end{aligned} \quad (2)$$

with the deformation potentials D_i and E_i . The E_i are assumed to be negligible, as is usually done in the literature^{10,15}.

The equivalent effective Hamiltonian for the Γ_6^+ conduction band is given by the 2×2 -matrix

$$\mathcal{H}_c(\mathbf{k}_e, \boldsymbol{\epsilon}) = E_g + \frac{\hbar^2}{2m_e} A_4 \mathbf{k}_e^2 + C_1 \text{Tr}(\boldsymbol{\epsilon}). \quad (3)$$

A spatially homogeneous strain preserves the inversion symmetry as well as the time-reversal symmetry. Thus, the twofold degeneracy over the whole Brillouin zone of both the Γ_7^+ valence band and the Γ_6^+ conduction band is maintained. As long as the strain field is approximately constant across the exciton volume, the assumption of spatial homogeneity is justified.

The kinetic energy of the relative electron-hole motion $\mathcal{H}_r(\mathbf{k}, \boldsymbol{\epsilon}) = \mathcal{H}_c(\mathbf{k}, \boldsymbol{\epsilon}) \otimes \text{Id}_v - \text{Id}_c \otimes \mathcal{H}_v(\mathbf{k}, \boldsymbol{\epsilon})$ for vanishing center-of-mass momentum $\hbar\mathbf{K} = 0$ is thus given by the 12×12 matrix

$$\mathcal{H}_r(\mathbf{k}, \boldsymbol{\epsilon}) = \text{Id}_c \otimes (E_g - \mathcal{H}_v(\mathbf{k}, \boldsymbol{\epsilon})) \quad (4)$$

with modified parameters $A_1 \mapsto A_1 - A_4$ and $D_1 \mapsto D_1 - C_1 := D'_1$. Here, Id_c and Id_v denote the identity matrices in the basis of conduction-band and valence-band states, respectively. This formulation is possible as $\mathcal{H}_c(\mathbf{k}_e, \boldsymbol{\epsilon})$ is proportional to Id_c and the terms in $\mathcal{H}_v(\mathbf{k}_h, \boldsymbol{\epsilon})$ containing A_1 and D_1 are proportional to Id_v .

The excitonic strain potential can be broken down into a pure band-gap shift ΔE_g and a binding energy shift ΔE_b induced by the deformation of the bands (for nS orthoexcitons not considered here, there is an additional strain-dependent contribution from the exchange interaction¹⁰). The band-gap shift ΔE_g can be evaluated in third-order perturbation theory as

$$\begin{aligned} \Delta E_g(\boldsymbol{\epsilon}) = & -D'_1 \text{Tr}(\boldsymbol{\epsilon}) - \frac{2D_3^2 [\epsilon_{xy}^2 + \epsilon_{yz}^2 + \epsilon_{zx}^2]}{3\Delta} - \frac{D_2^2 [(\epsilon_{xx} - \epsilon_{yy})^2 + (\epsilon_{yy} - \epsilon_{zz})^2 + (\epsilon_{zz} - \epsilon_{xx})^2]}{9\Delta} \\ & - \frac{D_2^3 (\epsilon_{xx} + \epsilon_{yy} - 2\epsilon_{zz})(\epsilon_{xx} - 2\epsilon_{yy} + \epsilon_{zz})(-2\epsilon_{xx} + \epsilon_{yy} + \epsilon_{zz})}{27\Delta^2} + \frac{2D_3^3 \epsilon_{xy} \epsilon_{yz} \epsilon_{zx}}{\Delta^2} \\ & + \frac{D_2 D_3^2 [\epsilon_{xx}(\epsilon_{xy}^2 + \epsilon_{zx}^2 - 2\epsilon_{yz}^2) + \epsilon_{yy}(\epsilon_{xy}^2 + \epsilon_{yz}^2 - 2\epsilon_{zx}^2) + \epsilon_{zz}(\epsilon_{zx}^2 + \epsilon_{yz}^2 - 2\epsilon_{xy}^2)]}{3\Delta^2}. \end{aligned} \quad (5)$$

For a compressive strain with $\text{Tr}(\boldsymbol{\epsilon}) < 0$, the first-order term raises the band gap and thus results in a repulsive contribution to the excitonic potential while the second-order terms lower the band gap.

III. BAND-GAP SHIFTS UNDER THE INFLUENCE OF STRAIN FROM A CYLINDRICAL STRESSOR

For some geometries, the stress field can be calculated analytically using Hertzian contact theory. It should be

TABLE I. Material properties of Cu₂O used in this work.

D'_1	2.1 eV		A_1	-1.76	
D_2	-3.9 eV	20	A_2	4.519	
D_3	1.9 eV		A_3	-2.201	5
S_{11}	41.69 TPa ⁻¹		B_1	0.02	
S_{12}	-19.36 TPa ⁻¹	18	B_2	-0.022	
S_{44}	82.64 TPa ⁻¹		B_3	-0.202	
ϵ_r	7.5	21	Δ	131 meV	2
A_4	1.01	22	E_g	2.17208 eV	3

noted here that Hertzian contact theory assumes elastically isotropic materials. However, comparisons between finite-element calculations and Hertzian results for germanium (whose anisotropy is stronger than that of Cu₂O) have shown satisfying agreement²³.

In the case of an infinitely long cylindrical stressor in contact with a planar surface along the x' axis of the (x', y') -plane (see Fig. 1), the components of the stress tensor $\sigma_{i'j'}$ are given by^{17,24}

$$\sigma_{x'x'} = -2\nu\hat{\sigma}[m - \tilde{z}'], \quad (6)$$

$$\sigma_{y'y'} = -\hat{\sigma} \left[m - 2\tilde{z}' + m \frac{\tilde{z}'^2 + n^2}{m^2 + n^2} \right], \quad (7)$$

$$\sigma_{z'z'} = -\hat{\sigma} \left[m - m \frac{\tilde{z}'^2 + n^2}{m^2 + n^2} \right], \quad (8)$$

$$\sigma_{y'z'} = \hat{\sigma} \left[n \frac{m^2 - \tilde{z}'^2}{m^2 + n^2} \right], \quad (9)$$

$$\sigma_{x'y'} = \sigma_{z'x'} = 0, \quad (10)$$

where $\hat{\sigma}$ is the maximum stress at the contact surface, $(\tilde{x}', \tilde{y}', \tilde{z}')^T = b^{-1}(x', y', z')^T$ are the dimensionless coordinates of the stress field and m and n are given by

$$m = \frac{\tilde{z}'}{\sqrt{2}|\tilde{z}'|} \left\{ (1 - \tilde{y}'^2 + \tilde{z}'^2) + \sqrt{(1 - \tilde{y}'^2 + \tilde{z}'^2)^2 + 4\tilde{y}'^2\tilde{z}'^2} \right\}^{\frac{1}{2}}, \quad (11)$$

$$n = \frac{\tilde{y}'}{\sqrt{2}|\tilde{y}'|} \left\{ (\tilde{y}'^2 - 1 - \tilde{z}'^2) + \sqrt{(1 - \tilde{y}'^2 + \tilde{z}'^2)^2 + 4\tilde{y}'^2\tilde{z}'^2} \right\}^{\frac{1}{2}}. \quad (12)$$

In the case of compressive stress, the sign of $\hat{\sigma}$ coincides with the sign of \tilde{z}' . The parameters $\nu = -S_{12}/S_{11} = 0.464$ and $Y = 1/S_{11} = 23.99$ GPa (see Table I) are Poisson's ratio and Young's modulus, respectively, and

$$b = 2|\hat{\sigma}|R(\Theta_{\text{Cu}_2\text{O}} + \Theta_{\text{stressor}}) \quad (13)$$

is the half width of the contact area between stressor and crystal, with the stressor's radius R and $\Theta = (1 - \nu^2)/Y$.

The line load F in Fig. 1 is related to the stress $\hat{\sigma}$ by

$$F = \frac{\hat{\sigma}\pi b}{2} = \pi\hat{\sigma}|\hat{\sigma}|R(\Theta_{\text{Cu}_2\text{O}} + \Theta_{\text{stressor}}). \quad (14)$$

Due to the elastic anisotropy of Cu₂O, the stress tensor $\boldsymbol{\sigma}(\mathbf{r})$ has to be transformed into the crystal coordinates $x \hat{=} [100]$, $y \hat{=} [010]$ and $z \hat{=} [001]$ first, before the strain tensor $\boldsymbol{\epsilon}(\mathbf{r})$ is calculated from it. The components of strain tensor and stress tensor are then connected by the compliance constants

$$\epsilon_{xx} = S_{11}\sigma_{xx} + S_{12}(\sigma_{yy} + \sigma_{zz}), \quad (15)$$

$$\epsilon_{yz} = S_{44}\sigma_{yz}/2 \quad (16)$$

for the diagonal and off-diagonal components, respectively (the other components are given by cyclic permutations).

Figure 2 shows the band-gap shifts for different orientations of the crystal relative to the stressor and a maximum stress of $\hat{\sigma} = -0.65$ GPa. The spatial splitting of the band-gap potential well for a main stress in $z' \hat{=} [011]$ direction viewed from $x' \hat{=} [100]$ (Fig. 2 (c)) has already been observed experimentally for spherical stressors¹⁰. For the cases shown in Fig. 2 (a), (b) and (d), the potential is well approximated by a harmonic potential in y' -direction, and is Morse-like along the z' -direction.

Figure 3 shows the range of stresses in which a potential minimum can form for the arrangement of Fig. 2 (a). The limiting factor for the formation of a trap is the minimum in the z' -direction, which only forms for stresses $|\hat{\sigma}| \gtrsim 0.25$ GPa. From the second derivatives at the trap minimum \mathbf{r}_{min} , the trap frequencies can be calculated as

$$\omega_{x_i} = \sqrt{\frac{1}{M} \frac{\partial^2 \Delta E_g(\mathbf{r})}{\partial x_i^2} \Big|_{\mathbf{r}=\mathbf{r}_{min}}} \quad (17)$$

where $M = (A_4^{-1} + (2B_1 - A_1)^{-1}) m_e = 1.55 m_e$ is the exciton mass and $x_i = y', z'$.

The trap frequencies for a stressor with $R = 0.5$ mm, $Y = 75$ GPa and $\nu = 0.3$ are shown in Fig. 4. For fixed $\hat{\sigma}$, the frequencies scale as $\omega \propto b^{-1} \propto R^{-1}(\Theta_{\text{Cu}_2\text{O}} + \Theta_{\text{stressor}})^{-1}$. The results in Fig. 3 have been obtained by a complete diagonalisation of $\mathcal{H}_r(0, \boldsymbol{\epsilon})$, as the perturbation theoretical treatment introduces errors of ~ 2 meV at the trap minimum for $\hat{\sigma} = -1$ GPa.

In order for the assumption of slowly varying strain to hold, the trap dimension should be much larger than the spatial dimension of the exciton states, i.e. $\langle r_{n,\ell} \rangle \ll b$. On the other hand, the excitonic lifetimes $\tau_{n,\ell}$ should be larger than the inverse trap frequencies ω^{-1} in order to have a meaningful definition of "trapped excitons". The inverse trap frequencies in our numerical example are on the same order of magnitude as the lifetimes of strain-free the Rydberg excitons $\tau_{n,\ell}$ that can be estimated from the FWHM linewidths^{3,25} $\hbar\gamma_{n,\ell} \approx \hbar/\tau_{n,\ell}$. This results in lifetimes on the order of 100 ps for the 15P states, compared to $\omega_x^{-1} \approx 500$ ps for the parameters used in Fig. 4. As

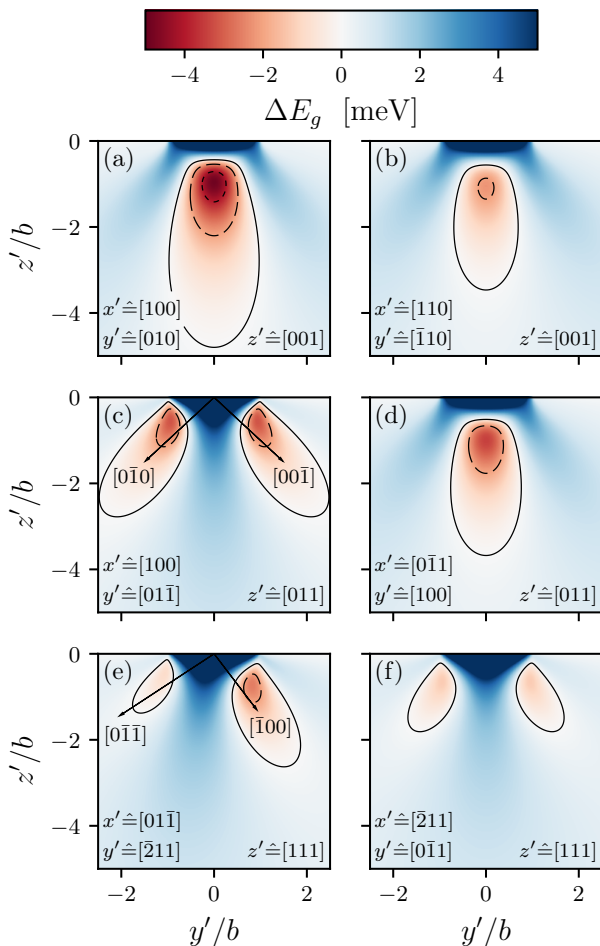


FIG. 2. Band-gap shifts ΔE_g for a maximum stress $\hat{\sigma} = -0.65$ GPa and different orientations of the stressor relative to the crystal axes. The contour lines mark the equipotential surfaces with $\Delta E_g = 0, -2, -4$ meV (solid, dashed, dotted). This representation does not depend on the stressor's material properties, its radius or the line load, as long as $\hat{\sigma}$ is kept fixed.

the trap frequency is inversely proportional to the trap dimension b , it can be tuned by the use of stressors with different radii. Additionally, strain is known to influence excitonic lifetimes in Cu_2O ²⁶. To the best of our knowledge no detailed studies on the influence of strain on the lifetimes of Rydberg excitons have been performed yet, which we will leave for future work.

In principle, much more intricate potential geometries can be created by corresponding stressors. As an example, Fig. 5 shows the approximate isosurfaces of the potential induced by a toroidal stressor pressed onto a Cu_2O crystal along the $[001]$ crystal axis and viewed along the $[110]$ direction. The isosurfaces were calculated under the assumption that the stressor is locally cylindrical. The modulation arises from the varying orientation of the stressor relative to the crystal axes (see Figs. 2 (a) and (b)).

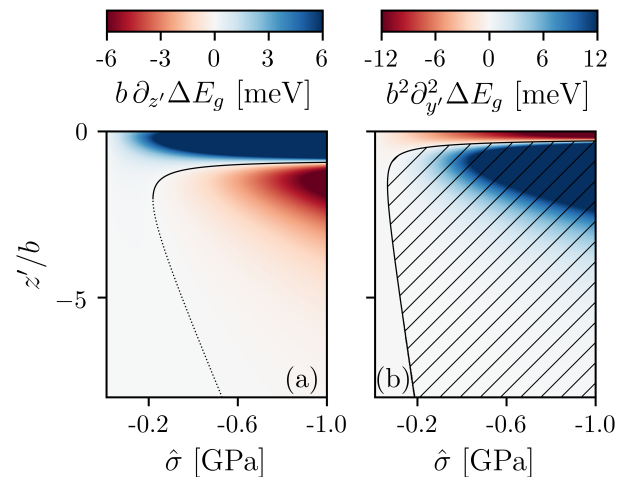


FIG. 3. Derivatives of ΔE_g for the geometry of Fig. 2 (a) and $y' = 0$. (a): Potential gradient in z' direction. The black lines mark the potential extrema, the upper branch (solid line) corresponds to the potential minimum. (b): Second derivative in y' direction. For symmetry reasons, the first derivative does always vanish in this configuration. ΔE_g has a minimum in y' -direction in the blue (hatched) region and a maximum in the red region.

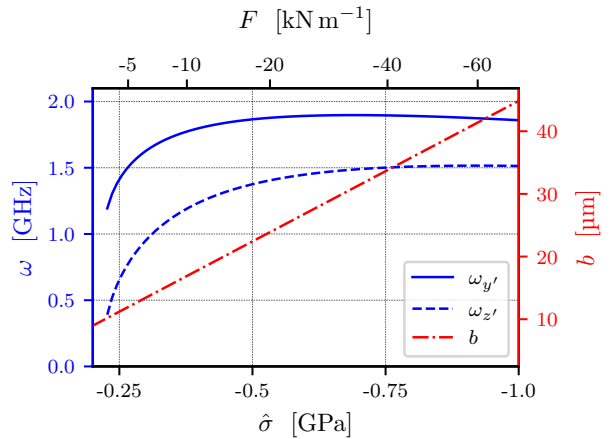


FIG. 4. Trap frequencies ω and contact half width b for a glass stressor with $R = 0.5$ mm, $Y = 75$ GPa and $\nu = 0.3$ in the arrangement of Fig. 2 (a).

IV. INFLUENCE OF STRAIN ON THE BINDING ENERGIES OF RYDBERG EXCITONS

As the excitonic states of interest in this study are odd-parity Rydberg states, the exchange interaction (which does not affect odd-parity states) and the coupling to the green exciton series via the kinetic Hamiltonian (4) (which should mostly affect states with large momentum space extension, i.e. small principal quantum number n) will be ignored. This enables the calculation of the exci-

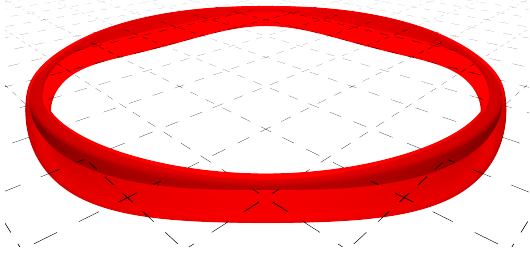


FIG. 5. Isosurfaces for $E = 0, -2$ meV (outer and inner surface, respectively) of the strain potential induced by a toroidal stressor pressed onto a Cu_2O crystal along the $[001]$ axis with $\hat{\sigma} = -0.65$ GPa. The radius (center of torus to center of contact area) was set to $\rho = 20b$, the grid lines are separated by $5b$.

tonic binding energies by solving the anisotropic Wannier equation of a spinless two-band model

$$[T(\mathbf{k}, \boldsymbol{\epsilon}) + V_{e-h}(\mathbf{k})\star] \phi(\mathbf{k}) = E\phi(\mathbf{k}) \quad (18)$$

with the convolution operator of the momentum-space Coulomb potential^{5,27} $V_{e-h}(\mathbf{k})$

$$V_{e-h}(\mathbf{k})\star\phi(\mathbf{k}) = \frac{1}{(2\pi)^{3/2}} \int d^3\mathbf{k}' V_{e-h}(\mathbf{k}-\mathbf{k}')\phi(\mathbf{k}') \quad (19)$$

and one eigenvalue $T(\mathbf{k}, \boldsymbol{\epsilon})$ of $\mathcal{H}_r(\mathbf{k}, \boldsymbol{\epsilon})$ corresponding to a product state of a hole in a Γ_7^+ state with an electron in a Γ_6^+ state. The approach to the solution of Eq. (18) used in this study is discussed in Appendix A.

In what follows, we will assume that the coordinates of the stress field x', y' and z' coincide with the crystal axes x, y and z (see Fig. 2 (a)). At $y = 0$, the strain becomes biaxial along y and z which reduces the local symmetry to D_{2h} ²⁸. This does potentially lift all degeneracies in the spin-less two-band model as all irreducible representations of the single group are one-dimensional. For $y \neq 0$, the strain is still confined to the (y, z) -plane (i.e. $\epsilon_{xx} = \epsilon_{xy} = \epsilon_{zx} = 0$), but the local symmetry reduces even further to C_{2h} . For other orientations of the stressor relative to the crystal axes, the local symmetries might be different. The only symmetry that is conserved under all (spatially homogeneous) strains is the inversion symmetry. Far from the contact zone $|y'| \gg b \vee |z'| \gg b$, the strain field vanishes and the O_h symmetry is recovered.

Figure 6 shows the binding energy shifts calculated from the two-band model including all odd-parity basis functions up to $\ell_{max} = 25$ and $n_{max} = 30 + \ell$. The strain-induced shift in the binding energy ΔE_b is on the order of μeV for the Rydberg states. As the band-gap shift is on the order of meV, it is the dominant potential contribution for states with large n : $\Delta E(\mathbf{r}) \approx \Delta E_g(\mathbf{r})$. The energetical distance between adjacent states might become important if one tries to address specific states inside the trap. Due to finite laser spot-sizes, spectra will always contain a spatial average over the strain shifts in the region of the laser spot.

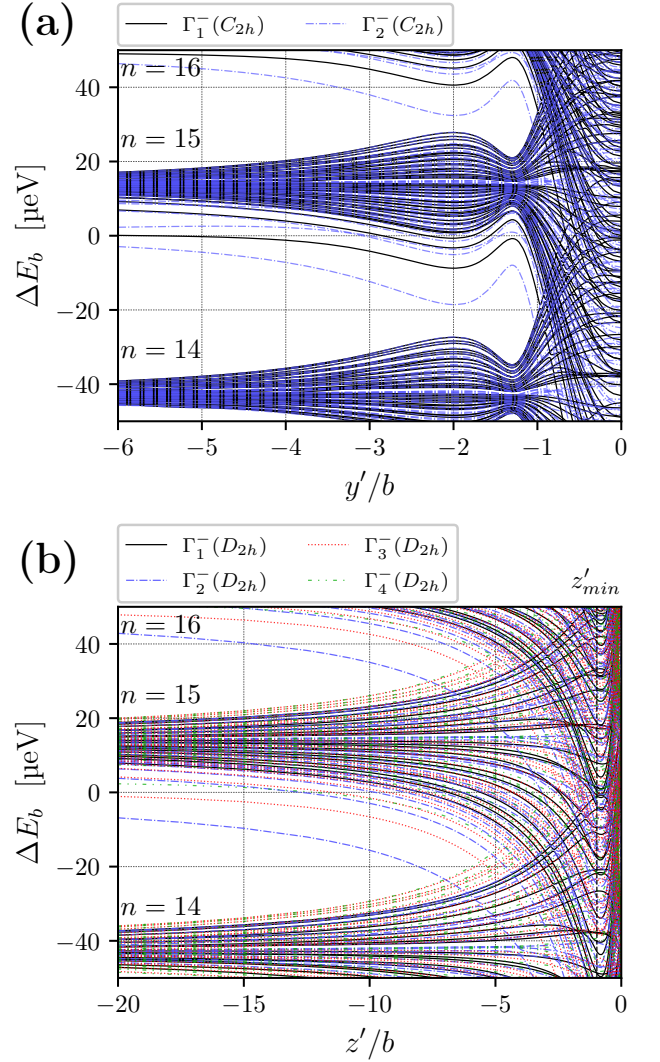


FIG. 6. Binding-energy shifts ΔE_b of the odd-parity excitons with $n = 14, 15$ and 16 relative to the strain-free $15P$ resonance ($E_b = -397$ μeV) for $\hat{\sigma} = -0.65$ GPa and the geometry of Fig. 2 (a). The energies are sampled along lines through the potential minimum parallel to the y' - and z' -axis, respectively. (a): $z' = z'_{min} = -0.95b$, (b): $y' = 0$.

The colors and linestyles denote the irreducible representations of the respective states and are the same as in Fig. 7.

For states with lower n , ΔE_b might reach the same order of magnitude as ΔE_g . This is shown in Fig. 7, which compares the shifts of the $2P$ resonances for the same conditions as in Fig. 6. In the region of the minimum of $\Delta E_g(\mathbf{r}_{min}) = -5.2$ meV, ΔE_b reaches values of -3.7 meV for $\Gamma_2^-(D_{2h})$, -1.3 meV for $\Gamma_3^-(D_{2h})$ and 3.4 meV for $\Gamma_4^-(D_{2h})$. The positions of the minima of the total potential $\Delta E_b + \Delta E_g$ differ slightly for the different symmetries, varying from $z' = -0.94b$ for $\Gamma_2^-(D_{2h})$ to $z' = -1.0b$ for $\Gamma_4^-(D_{2h})$.

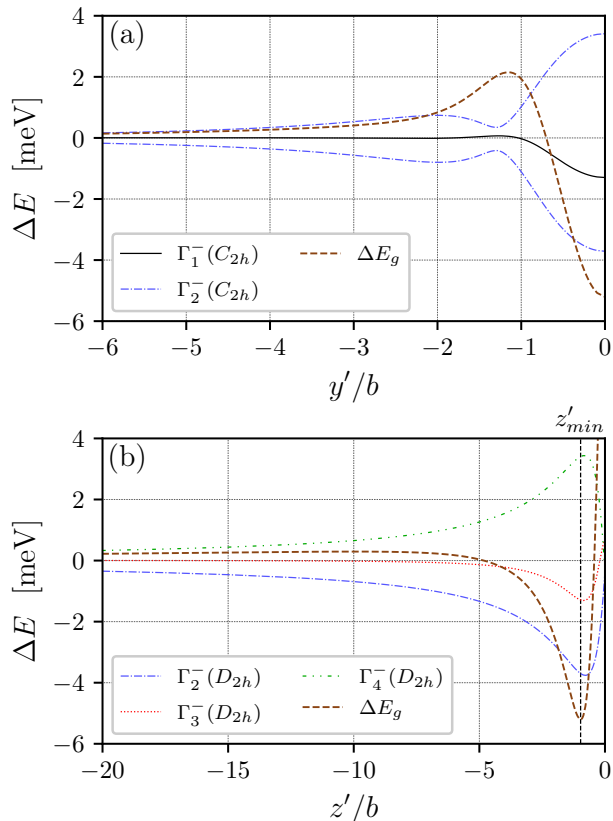


FIG. 7. Binding-energy shifts ΔE_b of the $2P$ resonances relative to the strain-free case ($E_b = -24.57$ meV) for the same conditions and with the same coding as in Fig. 6. The brown (dashed) line represents the band-gap shifts ΔE_g for comparison.

V. CONCLUSION AND OUTLOOK

We have shown that one can exploit the band-gap modification in a crystal to generate strain waveguides for Rydberg excitons that have similar or even superior parameters to optical dipole traps for atoms. For example, trap frequencies up to GHz and trap depths on the order of meV can potentially be reached. This implies that similar trapping geometries than those developed for atoms can be produced for excitons. The choice of stressor, together with the crystal orientation, determines the precise shape of the trapping potential with the possibility to create complex potential landscapes.

Our calculations have shown that, if one is only interested in the excitonic strain potential, it suffices to consider only the band-gap shift ΔE_g for the Rydberg states as it is about two orders of magnitude larger than the shift of the binding energies. The Rydberg states do, however, show a strong coupling, and potentially chaotic motion, in regions of high strain. Moreover, strain is known to influence the lifetime of excitons which will be the subject of future work.

ACKNOWLEDGMENTS

We acknowledge support by the Deutsche Forschungsgemeinschaft (DFG) via the Focussed Research Programme (SPP) 1929 'Giant Interactions in Rydberg systems'.

Appendix A: Numerical solution of the anisotropic two-band model

We will briefly review the numerical method used to compute the solutions of the isotropic, nonparabolic Wannier equation⁵, and extend it to anisotropic band structures. Starting point is the anisotropic momentum-space Wannier equation (18) written as a Sturmian eigenvalue problem

$$\left[\frac{\hbar^2 \mathbf{k}^2}{2\mu} + \Delta T(\mathbf{k}) - E \right] \Psi(\mathbf{k}) = -\lambda(E) V_{e-h}(\mathbf{k}) \star \Psi(\mathbf{k}) \quad (\text{A1})$$

with the anisotropic, nonparabolic part of the hole dispersion $\Delta T(\mathbf{k})$ and the reduced effective electron-hole mass μ , which both might depend on the strain tensor ϵ . In this calculation, however, the strain field is assumed to be constant over the extension of the exciton and those dependencies are not considered explicitly.

The Sturmian eigenvalues $\lambda(E)$ mark the excitonic eigenenergies $E_{n,\Gamma}$ by the condition $\lambda(E_{n,\Gamma}) = 1$. Hence, there is a parametric dependence of Eq. (A1) on the sought energy eigenvalue E which can be solved for the $\lambda(E)$ and the excitonic eigenenergies retrieved from them.

In contrast to Ref.⁵, $\Delta T(\mathbf{k})$ is no longer assumed to be isotropic, but may transform according to Γ_1^+ of O_h without strain and may retain only the inversion symmetry for arbitrary strain. In the strainless case, the exciton states split according to $S \mapsto \Gamma_1^+$, $P \mapsto \Gamma_4^-$, $D \mapsto \Gamma_3^+ \oplus \Gamma_5^+$ and $F \mapsto \Gamma_2^- \oplus \Gamma_4^- \oplus \Gamma_5^-$ in this model²⁹. Therefore, trial functions with the correct symmetries can be constructed as

$$\Psi_{\Gamma_j}(\mathbf{k}) = \sum_{\ell_\alpha} F_{\ell_\alpha}^{\Gamma_j}(k) \psi_{\ell_\alpha}^{\Gamma_j}(\mathbf{n}_k), \quad (\text{A2})$$

where $\psi_{\ell_\alpha}^{\Gamma_j}(\mathbf{n}_k)$ is the α th cubic harmonic³⁰ of order ℓ that transforms like a basis function Γ_j of the irreducible representation Γ , and $F_{\ell_\alpha}^{\Gamma_j}(k)$ is the corresponding radial wave function. In terms of the spherical harmonics $Y_\ell^m(\mathbf{n}_k)$, the relevant real-valued cubic harmonics up to fifth order for $\Gamma_{4,z}^-$ and tenth order for Γ_1^+ are

$$\psi_{0_1}^{\Gamma_1^+} = Y_0^0, \quad (\text{A3})$$

$$\psi_{4_1}^{\Gamma_1^+} = \sqrt{\frac{5}{24}}(Y_4^4 + Y_4^{-4}) + \sqrt{\frac{7}{12}}Y_4^0, \quad (\text{A4})$$

$$\psi_{6_1}^{\Gamma_1^+} = \sqrt{\frac{7}{16}}(Y_6^4 + Y_6^{-4}) - \sqrt{\frac{1}{8}}Y_6^0, \quad (\text{A5})$$

$$\begin{aligned} \psi_{8_1}^{\Gamma_1^+} &= \sqrt{\frac{65}{384}}(Y_8^8 + Y_8^{-8}) + \sqrt{\frac{7}{96}}(Y_8^4 + Y_8^{-4}) \\ &\quad + \sqrt{\frac{33}{64}}Y_8^0, \end{aligned} \quad (\text{A6})$$

$$\begin{aligned} \psi_{10_1}^{\Gamma_1^+} &= \sqrt{\frac{187}{768}}(Y_{10}^8 + Y_{10}^{-8}) + \sqrt{\frac{11}{64}}(Y_{10}^4 + Y_{10}^{-4}) \\ &\quad - \sqrt{\frac{65}{384}}Y_{10}^0, \end{aligned} \quad (\text{A7})$$

$$\psi_{1_1}^{\Gamma_{4,z}^-} = Y_1^0, \quad (\text{A8})$$

$$\psi_{3_1}^{\Gamma_{4,z}^-} = Y_3^0, \quad (\text{A9})$$

$$\psi_{5_1}^{\Gamma_{4,z}^-} = Y_5^0, \quad (\text{A10})$$

$$\psi_{5_2}^{\Gamma_{4,z}^-} = \sqrt{\frac{1}{2}}(Y_5^4 + Y_5^{-4}). \quad (\text{A11})$$

Inserting the expansion into Eq. (A1) while simultaneously expanding

$$D(\mathbf{k}) := \frac{2\mu\Delta T(\mathbf{k})}{\hbar^2} = \sum_{\ell''_\alpha} D_{\ell''_\alpha}(k) \psi_{\ell''_\alpha}^{\Gamma_1^+}(\mathbf{n}_k), \quad (\text{A12})$$

yields

$$\begin{aligned} &\sum_{\ell'_\alpha} \left[(k^2 + q^2) \delta_{\ell_\alpha, \ell'_\alpha} + \sum_{\ell''_\alpha} D_{\ell''_\alpha}(k) C_{\ell_\alpha, \ell'_\alpha, \ell''_\alpha}^{\Gamma_j} \right] F_{\ell'_\alpha}^{\Gamma_j}(k) \\ &= \frac{2\lambda(q)}{\pi a_B k} \int_0^\infty dk' k' F_{\ell_\alpha}^{\Gamma_j}(k') Q_\ell \left(\frac{k^2 + k'^2}{2kk'} \right) \end{aligned} \quad (\text{A13})$$

after multiplication by $\psi_{\ell_\alpha}^{\Gamma_j^\dagger}(\mathbf{n}_k)$ and integration over the unit sphere (for details, see Ref.²⁷). Here, $Q_\ell(x)$ denotes the Legendre functions of the second kind, $q = \sqrt{2\mu|E|}/\hbar$ is the renormalised energy, $a_B = 4\pi\epsilon_0\epsilon_r\hbar^2/(\mu e^2)$ the excitonic Bohr radius and

$$C_{\ell_\alpha, \ell'_\alpha, \ell''_\alpha}^{\Gamma_j} = \oint d^2\mathbf{n}_k \psi_{\ell_\alpha}^{\Gamma_j^\dagger}(\mathbf{n}_k) \psi_{\ell''_\alpha}^{\Gamma_1^+}(\mathbf{n}_k) \psi_{\ell'_\alpha}^{\Gamma_j}(\mathbf{n}_k) \quad (\text{A14})$$

the coupling coefficients of the cubic harmonics, which can be evaluated in terms of Wigner 3-j symbols. Equation (A13) can be rewritten as

$$\begin{aligned} J_{\ell_\alpha}^{\Gamma_j}(k) &= \frac{2\lambda(q)}{\pi a_B} \sum_{\ell'_\alpha} \int_0^\infty dk' \left[\mathbf{T}_{\Gamma_j}^{-1}(k', q) \right]_{\ell_\alpha, \ell'_\alpha} J_{\ell'_\alpha}^{\Gamma_j}(k') \\ &\quad \times \frac{Q_\ell \left(\frac{k^2 + k'^2}{2kk'} \right)}{\sqrt{k^2 + q^2} \sqrt{k'^2 + q^2}} \end{aligned} \quad (\text{A15})$$

where

$$J_{\ell_\alpha}^{\Gamma_j}(k) = k \sqrt{k^2 + q^2} \sum_{\ell'_\alpha} [\mathbf{T}_{\Gamma_j}(k, q)]_{\ell_\alpha, \ell'_\alpha} F_{\ell'_\alpha}^{\Gamma_j}(k) \quad (\text{A16})$$

and

$$[\mathbf{T}_{\Gamma_j}(k, q)]_{\ell_\alpha, \ell'_\alpha} = \delta_{\ell_\alpha, \ell'_\alpha} + \sum_{\ell''_\alpha} \frac{D_{\ell''_\alpha}(k)}{k^2 + q^2} C_{\ell_\alpha, \ell'_\alpha, \ell''_\alpha}^{\Gamma_j}. \quad (\text{A17})$$

As in the case of an isotropic band structure, the k -dependent part of the integral kernel in Eq. (A15) can be expressed as²⁷

$$\begin{aligned} M_\ell(q, k, k') &= \frac{2}{\pi a_B} \frac{Q_\ell \left(\frac{k^2 + k'^2}{2kk'} \right)}{\sqrt{k^2 + q^2} \sqrt{k'^2 + q^2}} \\ &= \sum_{n_r=0}^\infty g_{n_r, \ell}(k, q) g_{n_r, \ell}(k', q) \end{aligned} \quad (\text{A18})$$

where

$$\begin{aligned} g_{n_r, \ell}(k, q) &= \ell! \sqrt{\frac{n_r!}{\pi a_B (n_r + 2\ell + 1)!}} \frac{(4qk)^{\ell+1}}{(q^2 + k^2)^{\ell+3/2}} \\ &\quad \times C_{n_r}^{(\ell+1)} \left(\frac{q^2 - k^2}{q^2 + k^2} \right) \end{aligned} \quad (\text{A19})$$

with the Gegenbauer polynomials $C_{n_r}^{(\alpha)}(x)$. The functions $g_{n_r, \ell}(k, q)$ are orthogonal with respect to the radial quantum number n_r ,

$$\int_0^\infty dk g_{n_r, \ell}(k, q) g_{n'_r, \ell}(k, q) = \delta_{n_r, n'_r} \frac{1}{q a_B (n_r + \ell + 1)}, \quad (\text{A20})$$

and they form a natural basis in which to expand the $J_{\ell_\alpha}^{\Gamma_j}(k)$ in order to solve Eq. (A15) numerically.

In the case of strain, the calculation is equivalent with the exception that the correct lattice harmonics have to be chosen as the angular expansion functions (e. g. those for the point groups C_{2h} and D_{2h} for the y' - and z' -directions in Sec. IV or C_i in the most general case). These can be constructed by comparing the coupling coefficients given by Koster²⁹ and the Clebsch-Gordan coefficients.

For D_{2h} , the odd-parity lattice harmonics are (with odd ℓ and the obvious limits on α)

$$\psi_{\ell_\alpha}^{\Gamma_1^-} = i \sqrt{\frac{1}{2}} (Y_\ell^{2\alpha} - Y_\ell^{-2\alpha}), \quad (\text{A21})$$

$$\psi_{\ell_\alpha}^{\Gamma_2^-} = i \sqrt{\frac{1}{2}} (Y_\ell^{2\alpha+1} + Y_\ell^{-(2\alpha+1)}), \quad (\text{A22})$$

$$\psi_{\ell_0}^{\Gamma_3^-} = Y_\ell^0, \quad (\text{A23})$$

$$\psi_{\ell_\alpha}^{\Gamma_3^-} = \sqrt{\frac{1}{2}} (Y_\ell^{2\alpha} + Y_\ell^{-2\alpha}), \quad (\text{A24})$$

$$\psi_{\ell_\alpha}^{\Gamma_4^-} = \sqrt{\frac{1}{2}} (Y_\ell^{2\alpha+1} - Y_\ell^{-(2\alpha+1)}). \quad (\text{A25})$$

For C_{2h} they can be expressed as

$$\psi_{\ell_{\alpha\pm}}^{\Gamma_1^-} = \sqrt{\pm \frac{1}{2}} (Y_\ell^{2\alpha} \pm Y_\ell^{-2\alpha}), \quad (\text{A26})$$

$$\psi_{\ell_0}^{\Gamma_1^-} = Y_{\ell}^0, \quad (\text{A27})$$

$$\psi_{\ell_{\alpha\pm}}^{\Gamma_2^-} = \sqrt{\mp \frac{1}{2}} \left(Y_{\ell}^{2\alpha+1} \pm Y_{\ell}^{-(2\alpha+1)} \right), \quad (\text{A28})$$

if the z -axis is chosen as the twofold rotation axis. For C_i every odd-parity function belongs to Γ_1^- .

The \mathbf{k} -space extension of the Rydberg states scales roughly as n^{-1} . Therefore, the most important terms for highly excited states in (A12) are those with $D_{l_{\alpha}}(k) \propto k^2$ for $k \rightarrow 0$, which is only fulfilled by terms of zeroth and second order for the Γ_7^+ band. Including only those quadratic terms, the problem at hand can be expressed as the anisotropic Kepler problem

$$\left[\frac{\hbar^2 k_x^2}{2m_x} + \frac{\hbar^2 k_y^2}{2m_y} + \frac{\hbar^2 k_z^2}{2m_z} + V_{e-h}(\mathbf{k}) \right] \phi(\mathbf{k}) = E\phi(\mathbf{k}). \quad (\text{A29})$$

For O_h -symmetry, there are no terms with $\ell = 2$ that transform like Γ_1^+ , and the effective mass at the zone center of the Γ_7^+ valence band is isotropic. Hence, the coupling between different ℓ is small and the ansatz (A2) can be truncated at low ℓ_{α} . Inside the traps, the effective mass is quite anisotropic and states of different ℓ couple strongly. Therefore, all odd-parity basis functions with $n_r = n - \ell - 1 \leq 29$ and $\ell \leq 25$ had to be included, in order for the calculation of the binding-energy shifts of the $n = 15$ resonances to converge (giving bases of up to ~ 5500 basis functions). As the number of basis states scales with n^2 , the algorithm becomes computationally very expensive and not feasible for $n \gtrsim 15$.

-
- * sjard.krueger@uni-rostock.de
- ¹ E. F. Gross and N. A. Karryev, Doklady Akademii Nauk SSSR **84**, 471 (1952).
 - ² E. F. Gross, Il Nuovo Cimento (1955-1965) **3**, 672 (1956).
 - ³ T. Kazimierczuk, D. Fröhlich, S. Scheel, H. Stolz, and M. Bayer, Nature **514**, 343 (2014).
 - ⁴ J. Thewes, J. Heckötter, T. Kazimierczuk, M. Aßmann, D. Fröhlich, M. Bayer, M. A. Semina, and M. M. Glazov, Physical review letters **115**, 027402 (2015).
 - ⁵ F. Schöne, S.-O. Krüger, P. Grünwald, H. Stolz, S. Scheel, M. Aßmann, J. Heckötter, J. Thewes, D. Fröhlich, and M. Bayer, Physical Review B **93**, 075203 (2016).
 - ⁶ P. Grünwald, M. Aßmann, J. Heckötter, D. Fröhlich, M. Bayer, H. Stolz, and S. Scheel, Physical review letters **117**, 133003 (2016).
 - ⁷ D. P. Trauernicht, J. P. Wolfe, and A. Mysyrowicz, Physical Review B **34**, 2561 (1986).
 - ⁸ D. W. Snoke and V. Negoita, Physical Review B **61**, 2904 (2000).
 - ⁹ N. Naka and N. Nagasawa, Physical Review B **65**, 075209 (2002).
 - ¹⁰ N. Naka and N. Nagasawa, Physical Review B **70**, 155205 (2004).
 - ¹¹ K. Yoshioka, E. Chae, and M. Kuwata-Gonokami, Nature communications **2**, 328 (2011).
 - ¹² H. Stolz, R. Schwartz, F. Kieseling, S. Som, M. Kaupsch, S. Sobkowiak, D. Semkat, N. Naka, T. Koch, and H. Fehske, New Journal of physics **14**, 105007 (2012).
 - ¹³ R. Schwartz, N. Naka, F. Kieseling, and H. Stolz, New Journal of Physics **14**, 023054 (2012).
 - ¹⁴ K. Iwamitsu, S. Aihara, A. Ota, F. Ichikawa, T. Shimamoto, and I. Akai, Journal of the Physical Society of Japan **83**, 124714 (2014).
 - ¹⁵ C. Sandfort, J. Brandt, C. Finke, D. Fröhlich, M. Bayer, H. Stolz, and N. Naka, Physical Review B **84**, 165215 (2011).
 - ¹⁶ R. Grimm, M. Weidemüller, and Y. B. Ovchinnikov, Advances in atomic, molecular, and optical physics **42**, 95 (2000).
 - ¹⁷ E. M'Ewen, Philosophical Magazine **40**, 454 (1949).
 - ¹⁸ M. H. Manghnani, W. S. Brower, and H. S. Parker, physica status solidi (a) **25**, 69 (1974).
 - ¹⁹ K. Suzuki and J. C. Hensel, Physical Review B **9**, 4184 (1974).
 - ²⁰ H.-R. Trebin, H. Z. Cummins, and J. L. Birman, Physical Review B **23**, 597 (1981).
 - ²¹ C. Carabatos, A. Diffiné, and M. Sieskind, Journal de Physique **29**, 529 (1968).
 - ²² J. W. Hodby, T. E. Jenkins, C. Schwab, H. Tamura, and D. Trivich, Journal of Physics C: Solid State Physics **9**, 1429 (1976).
 - ²³ R. S. Markiewicz, J. P. Wolfe, and C. D. Jeffries, Physical Review B **15**, 1988 (1977).
 - ²⁴ The original paper apparently contains a sign error in the definition of $\sigma_{x'x'}$ as the equations given there do not describe a plane strain, as claimed ($\epsilon_{x'x'} = Y^{-1} [\sigma_{x'x'} - \nu(\sigma_{y'y'} + \sigma_{z'z'})]$ for isotropic materials).
 - ²⁵ F. Schweiner, J. Main, and G. Wunner, Physical Review B **93**, 085203 (2016).
 - ²⁶ S. Denev and D. W. Snoke, Physical Review B **65**, 085211 (2002).
 - ²⁷ R. Szymtkowski, Annalen der Physik **524**, 345 (2012).
 - ²⁸ G. L. Bir and G. E. Pikus, *Symmetry and strain-induced effects in semiconductors*, Vol. 624 (Wiley New York, 1974).
 - ²⁹ G. F. Koster, J. O. Dimmock, R. G. Wheeler, and H. Statz, Properties of the 32-point groups (1963).
 - ³⁰ F. C. Von der Lage and H. A. Bethe, Physical Review **71**, 612 (1947).